



## INVESTIGATION OF FLEXURAL AND ELASTIC BUCKLING BEHAVIOR OF CELLULAR BEAMS

Alırza İlker AĞÖNEN<sup>1</sup>, Barış GÜNEŞ<sup>2\*</sup>, Dia Eddin NASSANI<sup>3</sup>

<sup>1</sup> Kahramanmaraş Sutcu Imam University, Department of Civil Engineering, Kahramanmaraş, Turkey

<sup>2</sup> Istanbul University-Cerrahpasa, Department of Civil Engineering, Istanbul, Turkey

<sup>3</sup> Hasan Kalyoncu University, Department of Civil Engineering, Gaziantep, Turkey

### Keywords

Cellular Beam,  
Lateral Torsional Buckling,  
Elastic Buckling,  
Finite Element Analysis.

### Abstract

3D Finite Element Analysis (FEA) was performed to determine flexural and elastic lateral-torsional buckling behavior of cellular beam by using European steel shape and quality. An experimental study from literature was chosen for verification of the Finite Element Model (FEM). Parametric studies were carried out with a verified numerical model to investigate the effect of some geometrical properties of the cellular beam such as hole diameter, hole spacing, and various types of rigidity plates on elastic buckling and flexural capacity of the beam. Geometric and material nonlinear behavior were included in FEM. In the other part of the study, the theoretical calculation method of Lateral Torsional Buckling (LTB) with gross section and with net section properties was also investigated. The study showed that the LTB calculation method given by AISC360-16 and TSDC-2016 design guides provided more accurate result with net cross-section for European steel shapes and quality.

## DAİRESEL BOŞLUKLU KİRİŞLERDE EĞİLME VE YANAL BURULMALI BURKULMA DAVRANIŞININ İNCELENMESİ

### Anahtar Kelimeler

Dairesel Boşluklu Kiriş,  
Yanal Burulmalı Burkulma,  
Elastik Burkulma,  
Sonlu Eleman Analizi.

### Öz

Dairesel boşluklu kirişin eğilme ve elastik yanal burulmalı burkulma davranışını incelemek amacıyla Avrupa profilleri ve çelik kalitesi kullanılarak üç boyutlu sonlu eleman analizi gerçekleştirilmiştir. Literatürden bir deneysel çalışma sonlu eleman modelinin doğrulaması için seçilmiştir. Doğrulanmış sayısal model kullanılarak; delik çapı, delikler arası mesafe ve çeşitli tiplerde rijitlik levhası kullanımı gibi bazı geometrik özelliklerin kirişin eğilme ve elastik burkulma davranışını üzerindeki etkisini incelemek amacıyla parametrik çalışma yürütülmüştür. Sonlu eleman modeline malzeme ve geometrinin doğrusal olmayan davranışı dahil edilmiştir. Çalışmanın diğer bölümünde ise, yanal burulmalı burkulma teorik hesabı brüt ve net kesit özellikleri ile incelenmiştir. Sonuçlar, AISC360-16 ve TSDC-2016 tasarım rehberlerinde verilen hesaplama yönteminin net en-kesit özellikleri ile Avrupa profilleri ve çelik kalitesi için daha doğru sonuç verdiğini göstermiştir.

### Alıntı / Cite

Ağönen, A.İ., Güneş, B., Nassani, D.E., (2020). Investigation of Flexural and Elastic Buckling Behavior of Cellular Beams, Journal of Engineering Sciences and Design, 8(3), 869-882.

### Yazar Kimliği / Author ID (ORCID Number)

A.İ. Ağönen, 0000-0001-7384-8764  
B. Güneş, 0000-0003-1747-001X  
D.E. Nassani, 0000-0002-4196-8822

### Makale Süreci / Article Process

Başvuru Tarihi / Submission Date	18.03.2020
Revizyon Tarihi / Revision Date	04.08.2020
Kabul Tarihi / Accepted Date	05.08.2020
Yayın Tarihi / Published Date	24.09.2020

## 1. Introduction

Castellated beams with circular holes are named as cellular beams (AISC-31, 2017). Cellular beams are produced by cutting steel profiles using a computer-controlled torch. Cuts are made in a circular pattern. Separated two

\* İlgili yazar / Corresponding author: bgunes@istanbul.edu.tr, +90-532-748-8810

halves are welded back together from their webs to form a cellular beam. Castellated beams with various hole patterns are widely used in steel structures. Hole geometries are generally preferred as circular and hexagonal shapes. In recent years, usage of perforated beams with sinusoidal openings is also increasingly being used in steel framing systems. The cutting process of a beam with a hexagonal opening is performed in one pass, while the cellular beam is cut in two passes. Therefore, the cutting process for a cellular beam takes a longer time and the cellular beam manufacturing process produces more waste material than the beam with a hexagonal hole.

Cellular beams are widely applied in the roof and floor systems of structures that have wide openings and where the floor height should be limited (Parking structures, etc. Fig. 1) due to mechanical systems (ventilation, air conditioning, heating, etc.). They are also preferred in restoration works owing to its modern appearance.



**Figure 1.** Parking structure (Arcelormittal, 2020a)

The usage of the castellated beam provides a serious advantage for structure height. Perforated beam web decreases required structure height. A structure consists of 7 stories with ordinary beams can be built as an 8-story building with perforated beams. Thus, fewer stories decrease construction costs and construction time. Early completion of construction moves service time to earlier time. Beams that have a high moment of inertia decrease the need for the required column and foundation element quantity (Arcelormittal, 2020b). Lighter construction with fewer elements will be subjected to less earthquake load.

On the other hand, the stability problem (buckling) takes a very important place for steel perforated beam design. Parallel to advancing technology, material strength is increasing and required element cross-section size is decreasing. Furthermore, the effort to reduce construction weight to minimize construction material cost canalize design engineers to use thin-walled steel elements. Therefore, more attention has to be paid for the buckling problem of steel perforated beam. Elastic lateral-torsional buckling (LTB) can also be critical during the erection of steel structures. Perforated beams are generally preferred at large spans because of their increased carrying capacity. During erection, long perforated beams are subjected to its own dead load and worker live load before the installation of lateral beam supports. At this stage, the lateral movement of the compression flange is not prevented. This case most likely cause elastic lateral-torsional buckling (Bradley, 2003).

Numerical studies, parametric studies, and elastic buckling problems have attracted the attention of many researchers. (Akgöz and Civalek, 2017; Avcar, 2014a; Avcar, 2014b; Civalek and Kiracioglu, 2010). Extensive numerical, analytical, and experimental studies were found in the literature highlighting the flexural and elastic buckling behavior of cellular beams. Tsavdaridis and D'Mello (2011) conducted an experimental and analytical study on the behavior of perforated steel beams with closely spaced web openings. The finite element model (FEM) was established to investigate the effect of web opening spacing/web opening depth of web-posts and web opening depth/web thickness. An empirical formula was proposed to predict the ultimate vertical shear capacity of the web-post. Sweedan (2011) numerically investigated the lateral stability of the cellular beam. A 3D FEM with 2D shell elements was established. Effects of beam geometry and slenderness were studied on simply supported cellular beam which was subjected to various load types. Ellobody (2012) investigated nonlinear analysis of cellular steel beams under combined buckling modes. A 3D FEM with 2D shell elements was established which considers material nonlinearity, residual stress, and initial geometric imperfection of cellular beam. A parametric analysis also performed to study the effect of change in steel strength, cross-section geometry, and beam length on buckling behavior and capacity of cellular beam. Erdal and Saka (2013) ultimate load carrying capacities and finite element analysis of optimally designed steel cellular beams under loading conditions. Specimens were

optimally designed using harmony search method following BS5950 (2000). Experimental work and finite element analysis (FEA) were conducted with NPI profiles and S355 steel quality. El-Sawy et al., (2014) studied moment gradient factor of cellular steel beams under inelastic flexure. A 3D FEM with 2D shell elements was established. Simply supported cellular beam under various load types was considered. Parametric analysis is conducted to evaluate the effect of various geometrical properties on the inelastic stability of cellular steel beams. Pachpor et al., (2015) studied the behavior of cellular beam using design methods according to BS5950, considering the strength of the tee section and web-post element. A cellular beam was designed following BS5950 (2000) and the theoretical calculation result was compared with FEA for verification. Tsavdaridis and Galiatsatos (2015) conducted a parametric finite element analysis investigating closely spaced cellular beams with double concentric transverse stiffeners. Parameters such as (S/D) ratio, stiffener, and web thickness were investigated. Kwani and Wijaya (2017) studied LTB of castellated beams analyzed using the collapse analysis. FEM was analyzed by ADINA 8.9 (2013). At the end of the study, a correction factor for the AISC formula was offered to determine the critical moment of cellular beams. There are other studies in the literature where different types of steel elements are examined by FEA method (Pachideh et al., 2019; Yin et al., 2019; Jiang et al., 2019; Taheri et al., 2019; Roy et al., 2018; Roy and Lim, 2019).

As it is seen in the literature studies, most of the experimental studies on elastic buckling and flexural behavior of cellular beams were conducted with American wide flange steel profiles, American steel quality. Besides, 3D finite element studies presented in literature were conducted by using 2D shell elements. In this study, it was aimed to carry out more sensitive FEA with 3D solid elements for cellular beams to study flexural and elastic buckling behavior of beam by using European steel quality and European steel shapes. In addition, the validity of the theoretical calculation of critical LTB load for a cellular beam with both gross section and net section was studied by using European steel quality and European steel shapes.

**2. Material and Method**

**2.1. Verification Study**

Erdal and Saka (2013) conducted twelve experimental studies using NPI240, NPI260, and NPI280 steel profiles. S355 steel quality was preferred for all cellular beams. Specimens were supported as a simply supported beam with an approximately 3-meter span. The vertical force was applied at the mid-point of the beam. In this study, experimental study results conducted with the NPI240 profile is used for verification of FEA. Table 1 shows the dimensional properties of NPI240 based cellular beam and Table 2 ultimate load and failure mode of specimens reported by Erdal and Saka (2013).

**Table 1.** Dimensional properties of NPI 240 based cellular beam (mm) (Erdal and Saka, 2013)

H <sub>s</sub>	B <sub>f</sub>	T <sub>f</sub>	T <sub>w</sub>	D <sub>0</sub>	e	L
355.6	106,00	13,10	8,70	251,00	94,00	2.846,00

**Table 2.** Ultimate load capacities and failure modes of NPI\_240 sections (Erdal and Saka, 2013)

Specimens	Units	NPI240 Test1	NPI240 Test2	NPI240 Test3	NPI240 Test4
Ultimate loads	kN	270,50	273,70	284,10	286,20
Upper flange deflection (U_F_Def)	mm	4,29	3,79	13,89	14,15
Lower flange deflection (L_F_Def)	mm	3,36	3,39	12,99	13,20
Lateral deflection	mm	11,38	12,51	2,47	2,13
Failure mode		LTB	LTB	WPB	WPB

Test 1 and Test 2 graphics show that specimens laterally buckled around 200 kN or (M<sub>cr</sub>=140 kNm) before reaching ultimate bending capacity due to lack of lateral support. Arrows show the laterally buckled points of the specimens as illustrated in Fig. 2 and Fig. 3 As it is seen, LTB occurred in the elastic region. U\_F\_Def shows upper flange vertical deflection data, L\_F\_Def shows lower flange deflection data and Lat\_Def shows lateral movement measured using LVDT.

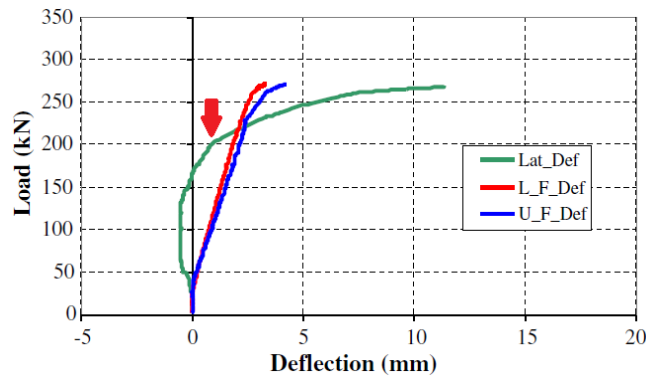


Figure 2. Load deflection graphics for NPI 240 (Test1) (Erdal and Saka, 2013)

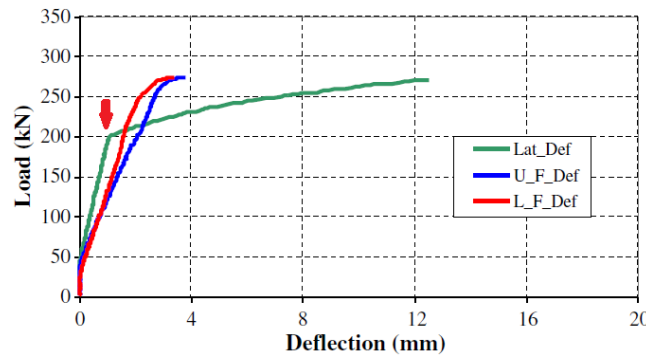


Figure 3. Load deflection graphics for NPI 240 (Test2) (Erdal and Saka, 2013)

### 2.2. Lateral Torsional Buckling (LTB) Behavior of Cellular Beams

LTB generates two kinds of stresses which are Saint Venant and Warping stresses. While Saint Venant stress occurs due to the rotation of section about a longitudinal axis, warping stress occurs due to the torsion of the section about a vertical axis (Timoshenko and Gere, 1961; Martini and Mohammad, 2011).

$$M_T = M_{SV} + M_W \tag{1}$$

$$M_{sv} = GJ \frac{d\phi}{dz} \tag{2}$$

$$M_w = -EC_w \frac{d^3\phi}{dz^3} \tag{3}$$

$$M_T = M_{SV} + M_W = GJ \frac{d\phi}{dz} - EC_w \frac{d^3\phi}{dz^3} \tag{4}$$

Solution of Equation of Equilibrium for laterally buckled case is given in the following equation.

$$EC_w \frac{d^4\phi}{dz^4} - GJ \frac{d^2\phi}{dz^2} - \frac{M_0^2}{EI_y} \phi = 0 \tag{5}$$

After the solution of differential equation considering boundary conditions, Critical Moment can be obtained as follows.

$$M_{ocr} = \frac{\pi}{L} \sqrt{EI_y GJ + \left(\frac{\pi E}{L}\right)^2 I_y C_w} \tag{6}$$

L is the laterally un-braced length for beam compression flange. E is the modulus of elasticity.  $I_y$  is the moment of inertia about the y-axis. G is the shear modulus, J is the polar moment of inertia and  $C_w$  is the warping constant.

$$M_n = C_b M_{ocr} \tag{7}$$

$$C_b = \frac{M_n}{M_{ocr}} \quad (8)$$

Previous calculation is valid for a beam which is subjected to fixed bending moment along its length. This is the most critical load case for LTB and may occur if the beam ends are subjected to the same amount of moment with opposite directions. However, beams may be exposed to various load types and moments during service life. Variation of moment along a beam length is considered by moment gradient factor ( $C_b$ ).  $C_b$  factor differs for some national steel design codes which are presented in Table 3 for mid-span concentrated load as follows.

**Table 3.** Moment gradient factor given by national design codes,  $C_b$  (Martini and Mohammad, 2011)

Loading Type	AISC360-16 (2016)	EC3 (2005)	AS4100 (1998)
Mid-Span Concentrated Load	1,32	1,37	1,35

Cross-section of beam elements that are subjected to bending moment can be classified as compact, non-compact, and slender according to AISC360-16 (2016) and TSDC-2016 (Turkish Steel Design Code, 2016). Geometric slenderness limitations are given in Table 4.

**Table 4.** Geometric Slenderness limitations (AISC360-16 (2016) and TSDC-2016 (2016))

Element	$\lambda$	$\lambda_p$	$\lambda_r$
Flange	$\frac{b_f}{2t_f}$	$0,38 \sqrt{\frac{E}{F_y}}$	$1,00 \sqrt{\frac{E}{F_y}}$
Web	$\frac{h}{t_w}$	$3,76 \sqrt{\frac{E}{F_y}}$	$5,70 \sqrt{\frac{E}{F_y}}$

After the Northridge Earthquake (1994), many experimental studies conducted in the USA to analyze damage occurred at steel structures. AISC 360-16 took its final form in the light of these experiences. American steel profiles (W profiles) and American steel quality (A992, A572 Gr. 50) were used in experimental studies. Turkish Steel Design Code (TSDC-2016) that came into force in 2016 seriously affected by AISC360-16. However, steel quality and steel shapes used in Turkey are quite different from the ones used in the USA. For this reason, a calculation conducted based on AISC360-16 with steel shape and steel quality used in Turkey. An experimental study conducted by Erdal and Saka (2013) with S355 steel quality and NPI240 steel profile was used for verification of the AISC360-16 design theory to determine LTB point. The effective radius of gyration ( $i_{ts}$ ) was calculated by using the following equation for gross and net section solution. Where  $b_f$  is flange width,  $t_f$  is the flange thickness,  $t_w$  is the web thickness and  $h$  is the height of the beam web.

$$i_{ts} = \frac{b_f}{\sqrt{12(1 + \frac{ht_w}{6b_f t_f})}} \quad (9)$$

Equation 9 considers the total cross-section area of beam flange and one-sixth of beam web height for calculation of an effective radius of gyration. LTB behavior of the prismatic beam is investigated based on preceding information given above according to AISC 360-16 and Turkish steel design code (TSDC-2016). These design codes state that the LTB problem for perforated beam can be examined using the gross section area of the beam. In this study, theoretical study results using gross-section and net section were compared with an experimental study results performed by Erdal and Saka (2013). Table 5 shows a comparison of critical LTB load with the net section and gross section. The verification study shows that LTB occurs around 200 kN ( $M_{cr}=140$  kNm) for cellular beam obtained from the NPI240 root profile. This result proves that LTB load calculation with gross section and net section overestimates the critical LTB capacity. For this reason, LTB load calculation with the net section and a more conservative safety factor (less than 0.9) is recommended by authors for design purposes.

**Table 5.** Hand Calculations with Gross and Net Section

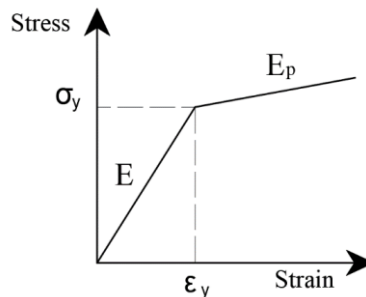
Properties	Units	Gross Section	Net Section
$A$ (area of the section)	$mm^2$	5.643,00	3.461,02
$J$ (torsional moment of inertia)	$mm^4$	234.044,20	175.897,90
$I_x$ (moment of inertia about $x$ )	$mm^4$	107.398.000,00	95.976.824,43
$I_y$ (moment of inertia about $y$ )	$mm^4$	2.618.460,00	2.604.680,00
$r_y$ (radius of gyration)	$mm$	21,50	27,43
$W_{ex}$ (elastic section modulus)	$mm^3$	604.038,00	539.802,16
$W_{px}$ (plastic section modulus)	$mm^3$	711.592,00	574.840,81
$L_p$ (Limiting laterally unbraced length for the limit state of yielding)	$mm$	899,87	1.146,01
$i_{ts}$ (effective radius of gyration)	$mm$	26,39	26,39
$h_o$ (Distance between flanges of beam)	$mm$	342,50	342,50
$L_r$ (Limiting laterally unbraced length for the limit state of inelastic lateral-torsional buckling)	$mm$	2.795,52	2.722,42
$C_b$ (Moment gradient factor)		1,32	1,32
$M_n$ (LTB moment)	$kNm$	178,04	152,22
$\phi M_n$ (Factored LTB moment)	$kNm$	160,24	137,00

## 2.3. Finite Element Model

### 2.3.1. Material Model and Material Properties

According to coupon tests given at the verification study, modulus of elasticity, yield strength, and ultimate rupture strength of steel were taken as 190.000,00 MPa, 390 MPa, and 495 MPa, respectively. Bilinear isotropic hardening material model (Fig. 4) was used in FEA. Tangent modulus in the plastic region was taken 1.000,00 MPa to prevent iteration problems (Akgönen et al., 2015). SOLID187 tetrahedral element with 10 nodes was selected which is well suited for irregular meshes (Sharcnet, 2017). SOLID187 element also has plasticity, large deflection, and large strain capabilities. Von Mises yield criteria (Beer et al., 2014), which are suitable for ductile materials, used to analyze stresses in the beam. When Von Mises stress ( $\sigma_{vm}$ ) value (equation 10) exceeds the yield capacity of material ( $\sigma_y > \sigma_{vm}$ ), the yield of material occurs.  $\sigma_x, \sigma_y, \sigma_z$  are normal stresses along  $x, y, z$  axes, respectively.

$$\sigma_{vm} = \frac{1}{\sqrt{2}} \sqrt{(\sigma_x - \sigma_y)^2 + (\sigma_y - \sigma_z)^2 + (\sigma_z - \sigma_x)^2} \quad (10)$$

**Figure 4.** Bilinear elasto-plastic material model

### 2.3.2. Boundary Conditions

The FEM was established as a simply supported beam model. Remote displacement command was used to apply boundary conditions. The following constraints were used for FEA. Table 6 shows the boundary conditions applied to the cellular beam and Fig. 5 shows X, Y, and Z directions.

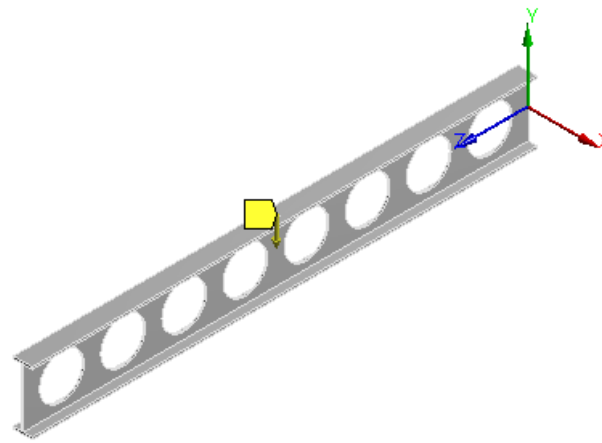


Figure 5. Axis used for boundary conditions

Table 6. Boundary conditions

Part	Translation			Rotation		
	x	y	z	r <sub>x</sub>	r <sub>y</sub>	r <sub>z</sub>
Left side	0	0	0	free	0	0
Right side	0	0	free	free	0	0

2.3.3. Investigation of Eigen-Value Problem by FEA

The rigidity matrix consists of elastic rigidity matrix [K<sub>E</sub>] and geometric rigidity matrix [K<sub>σ</sub>]. These matrixes are established automatically by ANSYS (2019). Buckling occurs when the total rigidity matrix equals to zero. This case is named as an Eigenvalue problem. The rigidity of bodies varies due to load type whether it is subjected to tension load or compression load. This variation is shown with [K<sub>σ</sub>] named as geometric rigidity matrix or initial stiffness matrix. [K<sub>σ</sub>] is a symmetric matrix that takes into account the increase or decrease of stiffness due to load type. The relationship between force and stiffness matrix for linear elastic finite element analysis is shown in equation 11. Where *F* is the force matrix applied to structure, *u* is the displacement matrix of nodes and λ is the eigenvalue. Buckling occurs when the rigidity matrix equals to zero (Martini and Mohammad, 2011).

$$\{F\} = [[K_E] + [K_σ] λ] \{u\} \tag{11}$$

Equation 12 (Martini and Mohammad, 2011) shows the total rigidity matrix of the structural element. 1 kN external vertical load was applied at mid-point of cellular beam to initiate elastic buckling analysis. Required lowest eigenvalue factor to solve rigidity matrix gives buckling load and related eigenvector gives buckling mode shape.

$$[[K_E] + [K_σ] λ] = 0 \tag{12}$$

2.3.4. Parametric Study

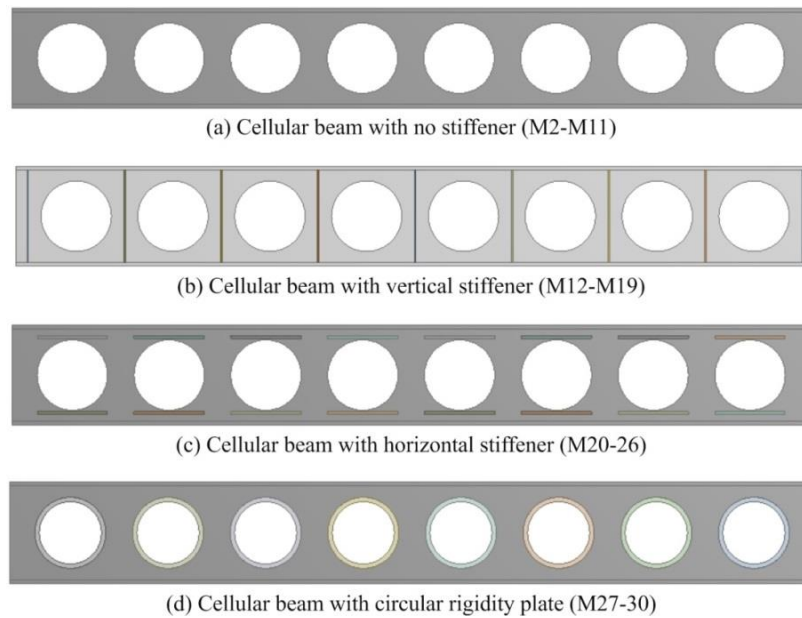
Four different types (Fig. 6) and seven different parameters were investigated in the parametric study. Firstly, (M1) was established (Fig. 6a) for verification of FEM which was obtained by the NPI240 root profile (Erdal and Saka (2013)) with 345 mm hole spacing and 251 mm hole diameter. Secondly, the hole diameter was varied for a fixed 345 mm hole spacing for M2-M7 models. Thirdly, hole spacing was varied for a fixed 251 mm hole diameter for M8-M11 models. Fourthly, vertical rigidity plates were placed (Fig. 6b) to verified model (M1) along web post centers for various thicknesses (M12-M15). Fifthly, vertical rigidity plate length was varied for vertical stiffener with 5 mm thickness (M16-M19). Sixthly, horizontal rigidity plates (Fig. 6c) were placed to verified model (M1) at 130mm above and below the center point of holes for various horizontal stiffener thicknesses (M20-M23). Seventhly, horizontal rigidity plate length was varied for vertical stiffener with 10 mm thickness (M23-M26). Lastly, a circular rigidity plate was added to the verified model (M1) for various circular rigidity plate thickness (M27-M30) (Fig. 6d). The geometrical properties of studied models can be seen in Table 7.

**Table 7.** Parametric study data

Model	s (mm)	D <sub>0</sub> (mm)	bvrp (mm)	tvrp (mm)	lvrp (mm)	bhrp (mm)	thrp (mm)	lhrp (mm)	bcrp (mm)	tcrcp (mm)
M1	345	251	-	-	-	-	-	-	-	-
M2	345	300	-	-	-	-	-	-	-	-
M3	345	200	-	-	-	-	-	-	-	-
M4	345	150	-	-	-	-	-	-	-	-
M5	345	100	-	-	-	-	-	-	-	-
M6	345	50	-	-	-	-	-	-	-	-
M7	345	0	-	-	-	-	-	-	-	-
M8	400	251	-	-	-	-	-	-	-	-
M9	450	251	-	-	-	-	-	-	-	-
M10	500	251	-	-	-	-	-	-	-	-
M11	550	251	-	-	-	-	-	-	-	-
M12	345	251	30	5	330	-	-	-	-	-
M13	345	251	30	8	330	-	-	-	-	-
M14	345	251	30	10	330	-	-	-	-	-
M15	345	251	30	12	330	-	-	-	-	-
M16	345	251	30	5	300	-	-	-	-	-
M17	345	251	30	5	275	-	-	-	-	-
M18	345	251	30	5	250	-	-	-	-	-
M19	345	251	30	5	200	-	-	-	-	-
M20	345	251	-	-	-	30	5	100	-	-
M21	345	251	-	-	-	30	8	100	-	-
M22	345	251	-	-	-	30	12	100	-	-
M23	345	251	-	-	-	30	10	100	-	-
M24	345	251	-	-	-	30	10	150	-	-
M25	345	251	-	-	-	30	10	200	-	-
M26	345	251	-	-	-	30	10	250	-	-
M27	345	251	-	-	-	-	-	-	60	5
M28	345	251	-	-	-	-	-	-	60	8
M29	345	251	-	-	-	-	-	-	60	10
M30	345	251	-	-	-	-	-	-	60	12

- s : spacing between holes.
- D<sub>0</sub> : hole diameter.
- bvrp : width of vertical rigidity plate.
- tvrp : thickness of vertical rigidity plate.
- lvrp : length of vertical rigidity plate.
- bhrp : width of horizontal rigidity plate.
- thrp : thickness of horizontal rigidity plate.
- lhrp : length of horizontal rigidity plate.
- bcrp : with of circular rigidity plate.
- tcrcp : thickness of circular rigidity plate

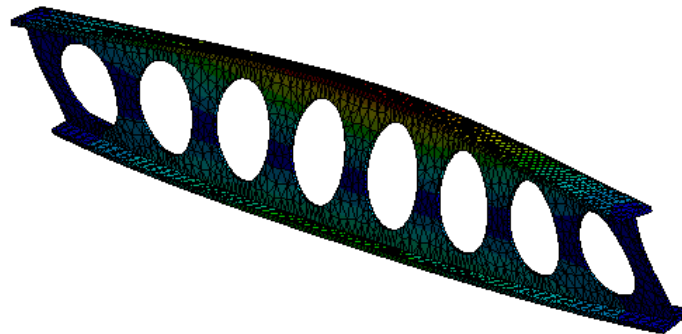




**Figure 6.** Studied cellular beam types

### 3. Results and Discussion

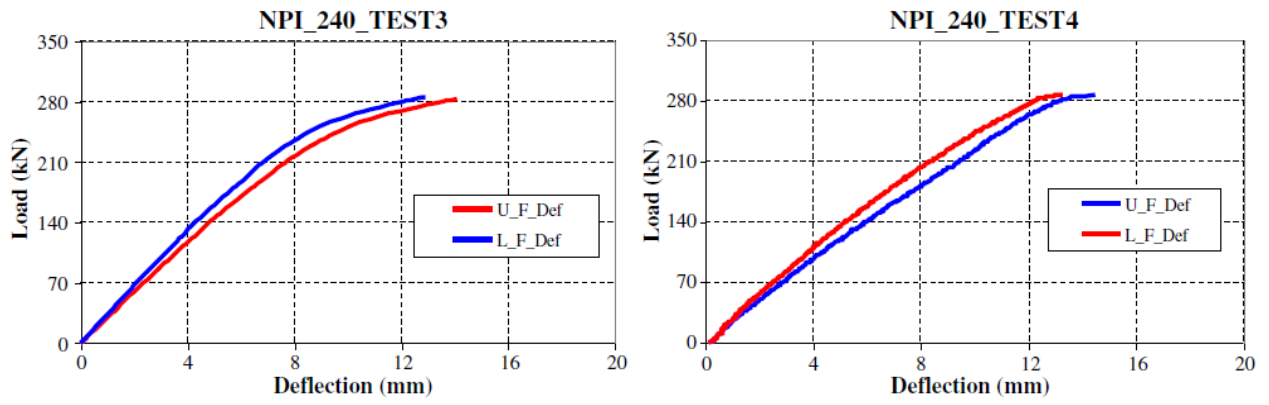
Finite element analysis was conducted to investigate the flexural and lateral-torsional buckling behavior of the cellular beam (Fig. 7). An experimental study from literature was chosen for verification of FEM. Parametric studies were performed with a verified numerical model to investigate the effect of some geometrical properties of the cellular beam such as hole diameter, hole spacing, and various types of rigidity plates on buckling and bending capacity of beams.



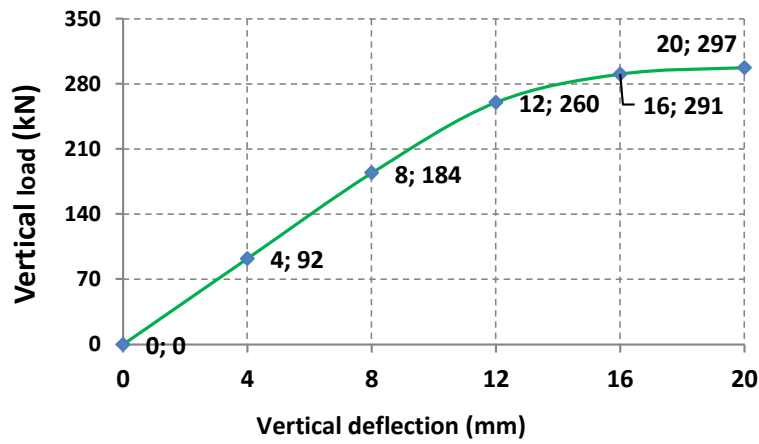
**Figure 7.** Laterally buckled shape of cellular beam

Fig. 8a shows the load-deflection curve of the experimental study for buckling-prevented specimens (Test3 and Test4) that reported by Erdal and Saka (2013) and Fig. 8b shows the FEA result. As it is seen, the FEA result suits well with experimental study results.

Fig. 9a shows the load-deflection behavior of cellular beam for various hole sizes. Center to center hole spacing was 345mm. Elastic rigidity and ultimate load capacity decreases due to hole size. Fig. 9b shows the ultimate load capacity-hole size relation for cellular beam. Maximum flexural capacity decreased almost linearly between D0-D200 models. A sudden capacity decrease was observed for D251 and D300. Ultimate load capacity decreased by 70% due to the increasing hole size compared to the no hole model. Fig. 9c shows vertical rigidity-hole size relation for cellular beam. Vertical rigidity was seriously affected by hole size for 150 mm or larger hole diameters. Vertical rigidity decreased 74% for D300 compared to D0. It was assumed that LTB was prevented to reach the ultimate flexural capacity of the cellular beam for Fig. 9a,b,c. Fig. 9d shows the ultimate elastic LTB load-hole diameter relation. Center to center hole spacing was 345mm. A parabolic decrease was observed due to the hole diameter increase. Elastic LTB capacity was not affected as much as the ultimate flexural capacity of the cellular beam. However, the 200 mm hole diameter can also be accepted as a critical value for LTB. LTB capacity for 300 mm hole diameter decreased 22,7% compared to the no hole model.

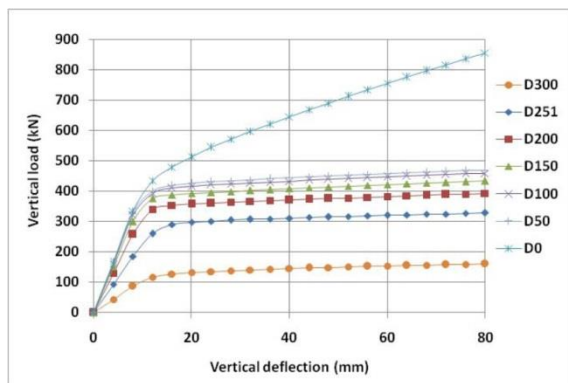


(a)

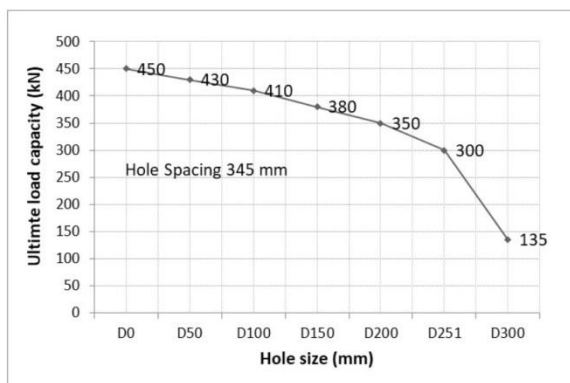


(b)

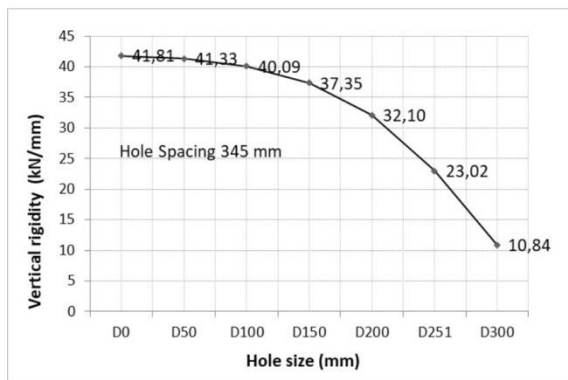
Figure 8. Comparison of Experimental study (Erdal and Saka, 2013) and FEA



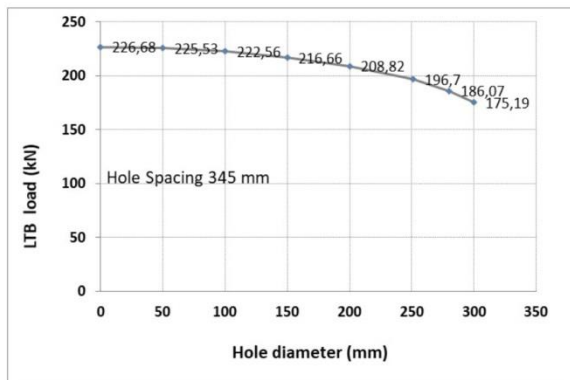
(a)



(b)



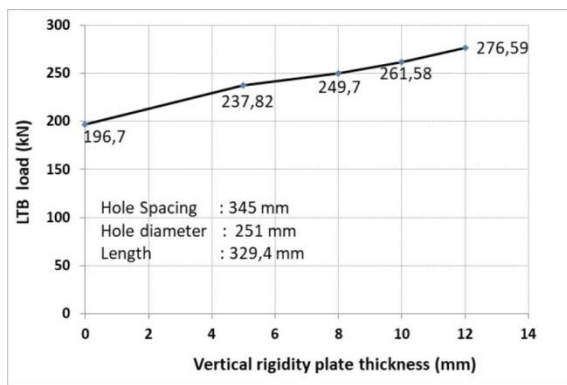
(c)



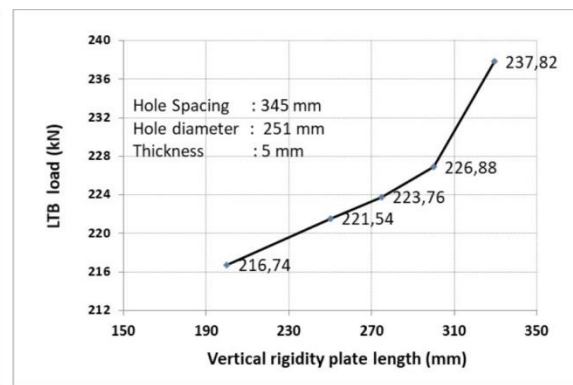
(d)

Figure 9. Graphics of parametric studies (1/2)

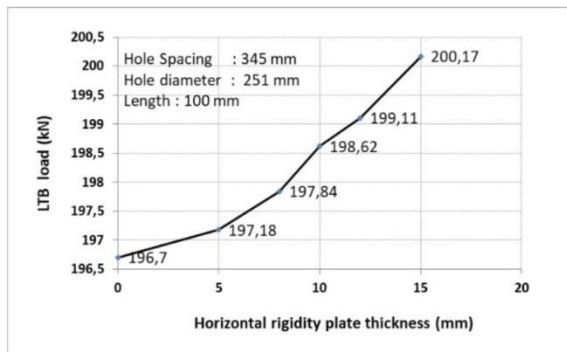
Fig. 10a shows the effect of vertical rigidity plate thickness on elastic LTB capacity. The length is 329,4 mm for all vertical rigidity plates. Almost a linear increase was observed due to the increase of vertical rigidity plate thickness. Vertical rigidity plate with 12 mm thickness (M15) increased the LTB capacity 40,6 % compared to the M1 model with no rigidity plate. Fig. 10b shows the effect of vertical rigidity plate length on elastic LTB capacity. Thickness is 5 mm for all rigidity plates. Vertical rigidity plate with 329,4 mm length increased LTB capacity up to 20,9% compared to the M1 model with no rigidity plate. Fig. 10c shows that horizontal rigidity plate thickness has a slight effect on LTB capacity. Rigidity plate with 15 mm thickness and 100 mm length increased LTB capacity around 2%. Fig. 10d shows the effect of horizontal rigidity plate length on elastic LTB capacity. Rigidity plate with 10 mm thickness and 250 mm length increased LTB capacity around 5,8% compared to the M1 model with no rigidity plate. Fig. 10e shows the effect of hole spacing on elastic LTB capacity. It was seen that elastic LTB capacity increased due to increased hole spacing. However, unexpected capacity decrease was observed for 500 mm hole spacing. Hole spacing affected the quantity of hole and the number of holes was also given in parenthesis. Fig. 10f shows the effect of circular rigidity plate thickness on elastic LTB capacity. Rigidity plate was used for all perimeter of hole (Fig. 6d). Circular rigidity plate with 12 mm thickness (M30) increased LTB capacity around 18,8% compared to the M1 model with no rigidity plate.



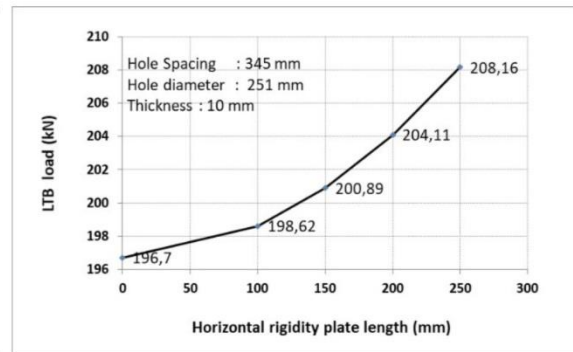
(a)



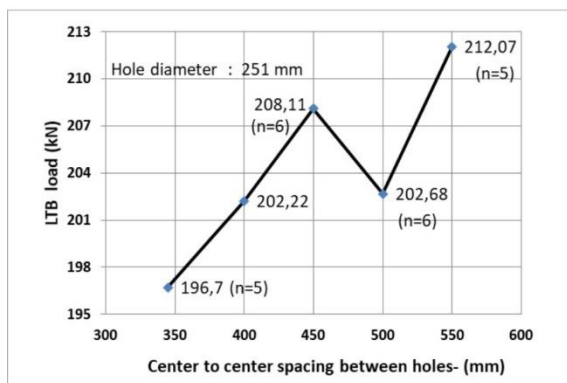
(b)



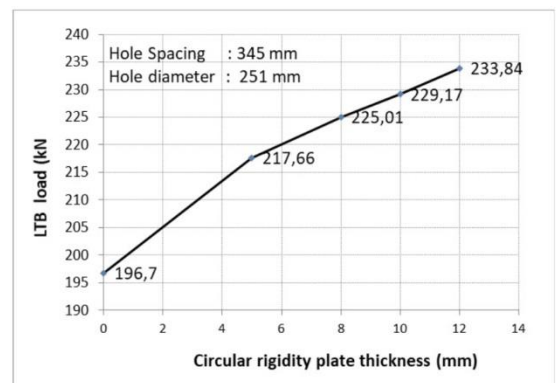
(c)



(d)



(e)



(f)

Figure 10. Graphics of parametric studies (2/2)

#### 4. Conclusions

3D finite element analysis was performed to determine the flexural and elastic lateral-torsional buckling behavior of a cellular beam. Parametric studies were performed with a verified numerical model to investigate the effect of some geometrical properties of the cellular beam such as hole diameter, hole spacing, and various types of rigidity plates on buckling and flexural capacity of beams. The major conclusions of this study are as follows.

- Usage of gross-section area is recommended to estimate the LTB capacity of cellular beam following AISC360-16 (2016) and TSDC-2016 (2016). Theoretical calculation of critical LTB load with gross-section area gave a larger result than the critical LTB load found at experimental work. However, critical LTB load obtained by using the net-section area with safety factor perfectly matched to experimental study result. More conservative safety factor and net cross-section area usage is recommended for safe cellular beam design.
- Most of the experimental studies on LTB were conducted with American wide flange steel profiles in literature. Theoretical calculations following AISC360-16 and TSDC-2016 showed good agreement with experimental and finite element study results conducted with European steel profiles and European steel quality. Effect of various hole geometries and various types of rigidity plates were studied on flexural and elastic LTB capacity of the cellular beam. Numerical studies showed that rigidity plates contribute significantly to LTB capacity depending on their type.
- Most of 3D finite element models were established using two-dimensional shell elements in the literature. In this study, a 3-D finite element model was established using three-dimensional SOLID187 tetrahedral elements with 10 nodes that provide higher sensitivity. Finite element analysis can satisfactorily predict both linear and non-linear flexural character of cellular beam with acceptable accuracy in terms of rigidity and ultimate beam flexural capacity. The finite element model showed satisfactory agreement to predict elastic buckling capacity and elastic buckling mode of the cellular beam.

#### Notation

The following symbols are used in this paper:

$A$	= area of the section
$B_f$	= spacing between holes
$D_o$	= hole diameter
$C_w$	= warping constant
$C_b$	= moment gradient factor
$E$	= modulus of elasticity
$G$	= shear modulus
$H_s$	= spacing between holes
$I_x$	= moment of inertia about x
$I_y$	= moment of inertia about y
$J$	= polar moment of inertia
$L$	= spacing between holes
$L$	= laterally un-braced length
$L_p$	= limiting laterally unbraced length for the limit state of yielding
$L_r$	= limiting laterally unbraced length for the limit state of inelastic lateral-torsional buckling
$M_{cr}$	= critical lateral torsional buckling moment under uniform bending
$\phi M_n$	= factored LTB moment subjected to specific transverse load
$M_n$	= LTB moment subjected to specific transverse load
$M_{ocr}$	= critical buckling moment acting in the plane of beam's web
$M_T$	= total torsional moment
$M_{SV}$	= Saint-Venant's pure torsion moment
$M_w$	= warping torsion component
$T_f$	= spacing between flange holes
$T_w$	= spacing between web holes
$W_{ex}$	= elastic section modulus
$W_{px}$	= plastic section modulus
$bcrp$	= width of circular rigidity plate

bf	= flange width
bhrp	= width of horizontal rigidity plate
bvrp	= width of vertical rigidity plate
e	= spacing between holes
h	= height of beam web
ho	= distance between flanges of beam
its	= effective radius of gyration
lhrp	= length of horizontal rigidity plate
lvrp	= length of vertical rigidity plate
ly	= length of vertical rigidity plate
tcrp	= thickness of circular rigidity plate
thrp	= thickness of horizontal rigidity plate
tvrp	= thickness of vertical rigidity plate
ry	= radius of gyration
s	= spacing between holes
tf	= flange thickness
tw	= web thickness
$\sigma_x$	= normal stresses along x axes
$\sigma_{vm}$	= Von Mises stress
$\sigma_y$	= normal stresses along y axes
$\sigma_z$	= normal stresses along z axes
$\epsilon$	= strain

### Conflict of Interest

No conflict of interest was declared by the authors.

### References

- ADINA 8.9, 2013. System Offers a Program for Comprehensive Finite Element Analyses of Structures. ADINA R & D, Inc.
- AISC-31. 2017. AISC Design Guide 31. Castellated and Cellular Beam Design. American Institute of Steel Construction. Chicago: American Institute of Steel Construction (AISC).
- Akgönen, A. İ., Yorgun, C., Vatanserver, C., 2015. Cyclic Behavior of Extended End-Plate Connections. *Steel and Composite Structures*, 19(5), 1185-1201.
- Akgöz, B., Civalek, B., 2017. A size-dependent beam model for stability of axially loaded carbon nanotubes surrounded by Pasternak elastic foundation. *Composite Structures*, 176, 1028-1038.
- ANSI/AISC 360-16, 2016. Specification for Structural Steel Buildings. American Institute of Steel Construction.
- ANSYS, 2019. Engineering Simulation & 3D Design Software.
- Arcelormittal, 2020a. Cellular Beams [https://constructalia.arcelormittal.com/files/5\\_4\\_1\\_Cellular\\_web--d7fedb749a4408ea2603fdd411761428.pdf](https://constructalia.arcelormittal.com/files/5_4_1_Cellular_web--d7fedb749a4408ea2603fdd411761428.pdf), accessed on July 2020
- Arcelormittal, 2020b. Cellular Beams. [http://sections.arcelormittal.com/fileadmin/redaction/4-Library/1-Sales\\_programme\\_Brochures/ACB/ACB\\_EN.pdf](http://sections.arcelormittal.com/fileadmin/redaction/4-Library/1-Sales_programme_Brochures/ACB/ACB_EN.pdf), accessed on January 2020
- AS4100, 1998. Australian steel standard.
- Avcar M., 2014a. Elastic Buckling of Steel Columns under Axial Compression. *American Journal of Civil Engineering*, 2(3), 102-108.
- Avcar M., 2014b. Free Vibration Analysis of Beams Considering Different Geometric Characteristics and Boundary Conditions. *International Journal of Mechanics and Applications*, 4 (3), 94-100.
- Beer, F. P., Johnston, E. R., DeWolf, J. T., Mazurek D. F. (2014). *Mechanics of materials*, 6th SI-Turkish Edition.
- Bradley, T. P., 2003. Stability of Castellated Beams. Msc. Thesis. Blacksburg, Virginia, United States of America.
- BS5950, 2000. British Standard Institution. London.
- Civalek, O., Kiracioglu, O., 2010. Free vibration analysis of Timoshenko beams by DSC method. *Int. J. Numer. Meth. Biomed. Engng.* 2010; 26:1890-1898.
- Ellobody, E., 2012. Nonlinear Analysis of Cellular Steel Beams Under Combined Buckling Modes. *Thin-Walled Structures*, 52, 66-79. doi:10.1016/j.tws.2011.12.009.
- El-Sawy, K. M., Sweedan, A. M., Martini, M. I., 2014. Moment Gradient Factor of Cellular Steel Beams under Inelastic Flexure. *Journal of Constructional Steel Research*, 98, 20-34. doi:10.1016/j.jcsr.2014.02.007
- EN 1993-1-1, 2005. Eurocode 3: Design of steel structures. The European Union.
- Erdal, F., Saka, M. P., 2013. Ultimate Load Carrying Capacity of Optimally Designed Steel Cellular Beams. *Journal of Constructional Steel Research*, 80, Pages 355-368. doi:10.1016/j.jcsr.2012.10.007
- Jiang, D., Xiao, C., Chen, T., Zhang, Y., 2019. Study on the Seismic Performance of Box-Plate Steel Structure with Openings Modular Unit. *Materials*, 12(24), 4142.
- Kwani, S., Wijaya, P. K., 2017. Lateral Torsional Buckling of Castellated Beams Analyzed Using the Collapse Analysis. *Journal of Constructional Steel Research*, 171, 813-820. doi:10.1016/j.proeng.2017.01.370
- Martini, H., Mohammad, M. I., 2011. Elasto-Plastic Lateral Torsional Buckling of Steel Beams with Perforated Web. Msc. Thesis. United Arab Emirates University.

- Pachideh, G., Gholhaki, M., Daryan, A., 2019. Analyzing the Damage Index of Steel Plate Shear Walls Using Pushover Analysis. *Structures*, 20, 437-451.
- Pachpor, P., Gupta, L., Deshpande, N., 2015. Analysis and Design of Cellular Beam and Its Verification. *IERI Procedia*, 7, 120-127. doi:10.1016/j.ieri.2014.08.019
- Roy, K., Lim, J., 2019. Numerical Investigation into the Buckling Behaviour of Face-To-Face Built-Up Cold-Formed Stainless Steel Channel Sections under Axial Compression. *Structures*, 20, 42-73.
- Roy, K., Ting, T., Lau, H., Lim, J., 2018. Effect of Thickness on The Behaviour of Axially Loaded Back-to-Back Cold-Formed Steel Built-up Channel Sections - Experimental and Numerical Investigation. *Structures*, 16, 327-346.
- Sharcnet, 2017. "Solid187":[https://www.sharcnet.ca/Software/Ansys/17.0/en-us/help/ans\\_elem/Hlp\\_E\\_SOLID187.html](https://www.sharcnet.ca/Software/Ansys/17.0/en-us/help/ans_elem/Hlp_E_SOLID187.html)
- Sweedan A.M.I., 2011. Elastic Lateral Stability of I-Shaped Cellular Steel Beams. *Journal of Constructional Steel Research*, 67, 182-194. doi:10.1016/j.jcsr.2010.08.009
- Taheri, E., Firouzianhaji, A., Usef, N., Mehrabi, P., Ronagh, H., Samali, B., 2019. Investigation of a Method for Strengthening Perforated Cold-Formed Steel Profiles Undercompression Loads. *Applied Science*, 9(23), 5085.
- Timoshenko, S., Gere, J., 1961, *Theory of Elastic Stability* (2nd b.). New York: McGraw-Hill.
- Tsavdaridis, K. D., D'Mello, C., 2011. Web Buckling Study of The Behaviour and Strength of Perforated Steel Beams With Different Novel Web Opening Shapes. *Journal of Constructional Steel Research*, 67, 1605-1620. doi:10.1016/j.jcsr.2011.04.004
- Tsavdaridis, K. D., Galiatsatos, G., 2015. Assessment of Cellular Beams with Transverse Stiffeners and Closely Spaced Web Openings. *Thin-Walled Structures*, 94, 636-650. doi:10.1016/j.tws.2015.05.005
- TSDC-2016., 2016. Regulation Regarding the Design, Calculation and Construction Basis of Steel Structures, Turkey: Minister of Environment and Urban Planning, Ankara.
- Yin, Z., Zhang, H., Yang, W., 2019. Study on Seismic Performance and Damage Analysis of Steel Plate Shear Wall With Partially Encased Composite (Pec) Columns. *Applied Science*, 9(5), 907.